JOURNAL OF COMPUTATIONAL PHYSICS 5, 415–442 (1970)

Propagation of a Shock Wave of Arbitrary Strength in Two Half Planes Containing a Free Surface*

RICHARD COLLINS AND HSIANG-TEH CHEN

Division of Applied Mechanics, Department of Engineering, University of California, Los Angeles, California 90024

Received November 11, 1969

The problem of propagation of an initially plane shock wave along a fluid interface is solved numerically, using the method of characteristics in conjunction with Whitham's technique. The results are limited to differences in shock velocity in the two fluid media of about 30% †. Greater degrees of shock diffraction will be accompanied by wave reflexions which have not been considered in Whitham's technique. The diffracted shock is found to be remarkably uniform, except in the vicinity of the free surface and the undisturbed shock, where it undergoes large changes in curvature.

I. INTRODUCTION

As a shock wave propagates through a general nonuniform medium in which the local sound speed varies with position, the shock will be diffracted, and its shape will become distorted. This is due to the fact that the varying fluid properties ahead of the shock front will cause some portions of the shock to change their velocity relative to adjacent segments. When a shock wave is diffracted, abrupt changes in shock shape are often accompanied by reflected waves which are necessary to assure that the general conservation relations remain satisfied across the distorted shock front.

The study of shock wave propagation in nonuniform media finds particularly important application in the oceans and upper atmospheres. Such shock or blast waves may be formed by vehicles traveling supersonically, or as a direct consequence of strong explosions.

In this work, we consider the problem of the diffraction of an initially plane normal shock front as it sweeps along a free interface separating two half-planes containing different homogeneous fluids at rest (Fig. 1.1).

Explicitly, we study the situation of a plane step-shock of Mach number M_0

* Presented at the Section on Numerical Methods in Gasdynamics of the Second International Colloquium on Gasdynamics of Explosions and Reacting Systems in Novosibirsk, USSR, August 19, 1969.

† *Note added in proof:* This restriction has since been removed by a generalized treatment at the interface.

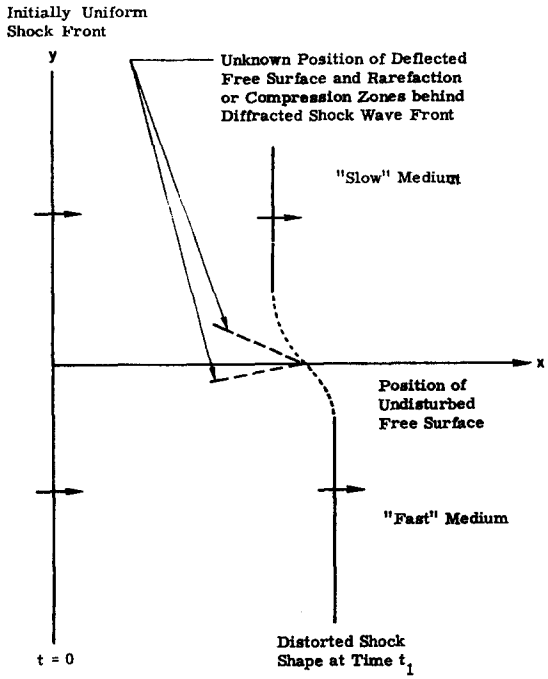

FIG. 1.1. Interaction of a plane shock front with a free surface separating two different fluids, each of semiinfinite extent.

which initially travels parallel to the axis $x = 0$ in the direction of increasing values of x. At time $t = 0$, the shock crosses the free interface ($y = 0$) separating a homogeneous fluid in the upper half-plane ($x > 0$, $y > 0$) from a different homogeneous fluid in the lower half-plane ($x > 0$, $y < 0$). The subsequent motion of the shock front is determined as it propagates through the two fluids. The interaction obtained depends on the initial speed of the shock relative to the sound speeds in each of the two media. The free interface will be displaced as a result of the varying pressure along the back surface of the shock front. The pressure and normal fluid velocity must be represented as continuous functions across this displaced interface, the true position of which is not known a priori.

The motion of the shock itself may be approximated by an extension of a method originally due to Chisnell [4] and reinterpreted by Whitham [18], in which disturbances to the motion of the shock are considered as constituting a wave motion on the shock itself. A curvilinear coordinate system is formed of a network consisting of successive shock wave positions and their orthogonal trajectories (*rays*). In this way, the flow field is divided up into a series of adjacent *ray*-tubes in which the cross-sectional area changes slowly with distance along the tube.

The simplifying assumption implied in the technique of Whitham is that the shock Mach number is a function of local cross-sectional area only. Thus, the effects of reflected waves behind the shock front which may in turn be re-reflected from the contact discontinuity and overtake the shock are neglected in this method. A relation, first developed by Chester ([2], [3]), is used to relate changes in shock Mach number to local changes in cross-sectional area of the ray tube.

The modified method of Whitham has been applied to an investigation of shock bifurcation in a heated layer on a flat plate by G. P. Talbot [7] in an effort to predict the time for formation of a second shock. The application of the technique to shock interaction with free surfaces is new. Additional complications arise in this case in the treatment of the boundary conditions at the distorted free surface which is no longer a *ray* as it would be were it a rigid surface.

The initial interaction of a uniform shock front with the two fluid domain is considered in Section II. The results of this study yield the strength of the transmitted shock fronts, whose subsequent diffraction and propagation are studied in the remainder of the work. Section III describes the mathematical formulation in terms of the method of Chisnell–Whitham. The numerical schemes adopted in the solution by the method of characteristics are explained in Section IV followed by the results and discussion and concluding remarks of Section V and VI.

Results have been calculated for a number of cases, but only one representative case, in which the shock speeds in the upper and lower media differ by 26%, is reported. There is evidence to believe that the degree of difference in shock speeds to which the technique of Whitham can be applied is limited, very likely due to an increasing contribution of reflections behind the shock front at the free surface.

II. Initial Interaction Between the Incident Shock and the Contact Surface

At time $t = 0$, the initially uniform shock front arrives at the interface separating two homogeneous fluids of different densities, and sound speeds (Fig. 1.1). The interaction will result in a transmitted shock front and a reflected wave which may be either of compression or expansion type. The method of distinguishing, a priori, between these two possibilities has been discussed in an excellent review article by Pack [13] as well as by Stocker and Butler [16] and by Courant and Friedrichs [6].

According to Pack, the nature of the reflected wave is governed by the ratio of the shock impedances, defined as the product of the equilibrium density and speed of the shock wave moving downstream through it. However, the velocity of the shock is of course not known a priori, rendering this criterion of little practical use. Instead of comparing shock impedances, we can compare the acoustic im-

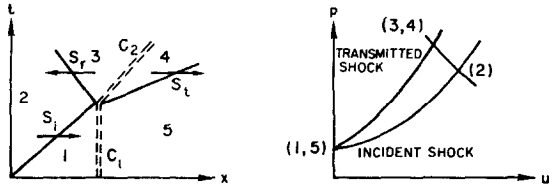

FIG. 2.1. Shock-contact surface interaction giving rise to reflected shock.

pedances. A shock wave is always reflected from a medium of greater shock impedance, or less correctly, acoustic impedance. By using the generalized expression for acoustic impedance A, a shock or a rarefaction wave will be reflected according as $A_i < A_t$ or $A_i > A_t$. It is possible to predict the character of a reflected wave of finite strength in this way.

If a shock wave is reflected; i.e., $A_t < A_i$ (see Fig. 2.1)

$$\frac{a_5\left(\frac{p_3}{p_1}-1\right)}{\gamma_t\sqrt{\frac{\gamma_t+1}{2\gamma_t}\frac{p_3}{p_1}+\frac{\gamma_t-1}{2\gamma_t}}}-\frac{a_1\left(\frac{p_2}{p_1}-1\right)}{\gamma_i\sqrt{\frac{\gamma_i+1}{2\gamma_i}\frac{p_2}{p_1}+\frac{\gamma_i-1}{2\gamma_i}}}=-\frac{a_2\left(\frac{p_3}{p_2}-1\right)}{\gamma_i\sqrt{\frac{\gamma_i+1}{2\gamma_i}\frac{p_3}{p_2}+\frac{\gamma_i-1}{2\gamma_i}}} \tag{2.1}$$

Equation (2.1) contains only one unknown quantity $p_3(=p_4)$, and this determines the strength of the reflected wave as well as the transmitted wave.

If a rarefaction wave is reflected; i.e., $A_i > A_t$ (see Fig. 2.2)

$$\frac{\left(\frac{p_3}{p_1}-1\right)\cdot a_5}{\gamma_t\sqrt{\frac{\gamma_t+1}{2\gamma_t}\left(\frac{p_3}{p_1}\right)+\frac{\gamma_t-1}{2\gamma_t}}}-\frac{\left(\frac{p_2}{p_1}-1\right)\cdot a_1}{\gamma_i\sqrt{\frac{\gamma_i+1}{2\gamma_i}\left(\frac{p_2}{p_1}\right)+\frac{\gamma_i-1}{2\gamma_i}}}=-\frac{2a_2}{\gamma_i-1}\left\{\left(\frac{p_3}{p_2}\right)^{(\gamma_i-1)/2\gamma_i}-1\right\}. \tag{2.2}$$

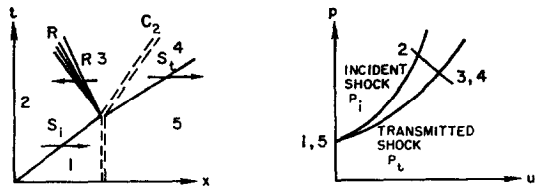

FIG. 2.2. Shock-contact surface interaction giving rise to reflected rarefaction.

Again, an equation is obtained for p_3, determining the strengths of the reflected and transmitted waves.

If the reflected wave is an acoustic wave, then $u_2 = u_3$ and $p_2 = p_3$. Both Eqs. (2.1) and (2.2) are identically equal to zero; i.e., they will yield the same strength of transmitted shock.

The relations derived above have been obtained in different forms by Paterson [14] and by Gubanov [7].

With the strengths of the initial transmitted shocks now known from the above calculations, the more difficult problem remains of computing the diffraction of this shock front as it propagates through the two media.

III. Diffraction of the Transmitted Shock Front

The transmitted shock front will travel at different speeds in the upper and lower media as a result of the different sound speeds in these two media. Consequently, the initially uniform shock front must bend or diffract in order to adapt to the new flow conditions ahead of it.

The deformed shape of the shock front will be calculated for the general case of an incident shock wave of arbitrary strength propagating into two media of significantly different properties. Since the positions of the diffracted shock and distorted free surface are not known a priori, an analytic solution is not realizable.

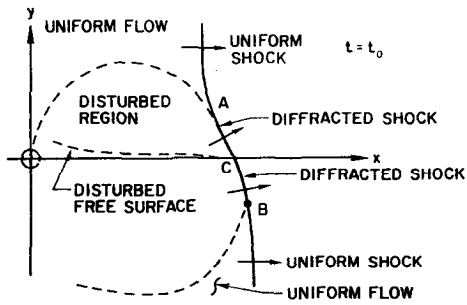

FIG. 3.1. Interaction between diffracted wave and shock wave.

The flow pattern behind the diffracting shock is shown on Figure 3.1 for the case in which the shock travels more rapidly in the lower plane, at a particular time $t_0 > 0$. The discussion applies, nonetheless, to the general case.

A discontinuity in shock inclination and shock strength will occur at the free surface as a result of the abrupt change in fluid properties. As a result, the pressure in the fluid behind the shock at point C will also suffer an abrupt discontinuity.

This will serve to displace the free surface to one side of its initial horizontal position, so that the conditions of continuity of pressure and normal velocity are again restored. In addition, at the points A and B, a wave will be reflected as a result of the rapid change of curvature of the diffracted shock as it rejoins the uniform shock. This reflected wave becomes in fact the first carrier of the disturbance created by the free surface into the upper and lower half planes of the fluid.

If one is interested primarily in the rate of propagation of the shock front and in its shape as a function of time, the problem may be reduced to an equivalent two-dimensional formulation in terms of distance along the shock and distance along rays which form normal trajectories between successive shock positions. The method idealizes the flow into a series of adjacent infinitesimal channels, whose cross-sectional area changes with distance along the channel. An area-Mach number relationship, first developed by Chester, is used which depends upon local flow conditions directly behind the shock wave. Thus wave reflexions due to interactions of the shock front with downstream contact discontinuities generated at earlier times are not accounted for.

A small area change in the duct will modify the strength of the transmitted shock in the following way:

$$\frac{dA}{A} = \frac{-2M\,dM}{(M^2 - 1)\,K(M)}, \tag{3.1}$$

where

$$K(M) = 2 \cdot \left[\left(1 + \frac{2}{\gamma + 1}\,\frac{1 - \mu^2}{\mu}\right)(2\mu + 1 + M^{-2})\right]^{-1} \tag{3.2}$$

and

$$\mu^2 = \frac{(\gamma - 1)\,M^2 + 2}{2\gamma M^2 - (\gamma - 1)}. \tag{3.3}$$

$K(M)$ is a very slowly varying (monotonic decreasing) function of shock Mach number, ranging from 0.5 for weak shocks ($\gamma = 1.4$) to 0.3941 for strong shocks. Chisnell suggests that the above relation could be integrated to provide a relation between shock Mach number and cross-sectional area even when the variations in duct area are not small. The resulting expression is very complex. If one ignores the small variation in $K(M)$, and evaluates this function for a mean value of the expected variation of M, then the area-Mach number relationship becomes simply

$$A^K(M^2 - 1) = \text{const.} \tag{3.4}$$

Whitham was able to reinterpret the results of Chisnell in terms of a simple rule. The equations of motion governing the fluid are written in characteristic form. Then the rule is to apply the characteristic relations to the flow quantities just behind the shock front, together with the shock relations. In this way, one deter-

mines the motion of the shock wave. The method has demonstrated remarkably high accuracy in a wide range of problems. The accuracy of the method will be discussed later for this particular problem.

It is convenient to consider a curvilinear coordinate system consisting of a network formed by successive shock wave positions on the one hand, and the orthogonal trajectory to successive shock positions on the other. The former are denoted in Figure 3.2 as lines of constant α(β-axes), and the latter as lines of

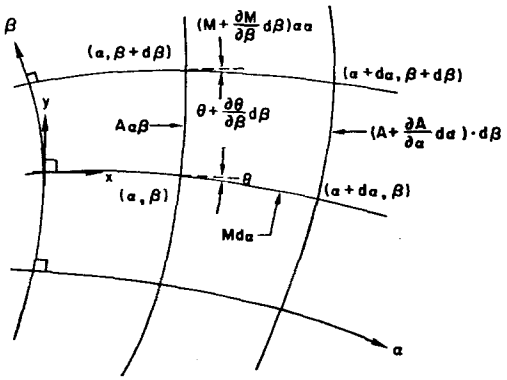

FIG. 3.2. Curvilinear coordinate system.

constant β(α-axes). If the fluid is at rest ahead of the shock front, then fluid particles will be propelled forward in the direction of motion of the shock front as it sweeps past; that is, the fluid motion relative to a fixed observer, will be directed normal to the shock front. The orthogonal *rays* normal to successive shock positions may then be considered as the boundary walls of an infinitesmal channel.

The following geometric relationships, which may be derived most generally from the condition of the flatness of the geometric space, then follow for the curvilinear coordinate system of Figure 3.2.

$$M(\partial\theta/\partial\beta) = \partial A/\partial\alpha \tag{3.5}$$

$$\partial M/\partial\beta = -A(\partial\theta/\partial\alpha), \tag{3.6}$$

where θ is the inclination of the normal to the shock with a fixed direction, M is the shock Mach number and A is the cross-sectional area of the elemental channel. Using (3.4), the Eqs. (3.5) and (3.6) become

$$\frac{\partial\theta}{\partial\alpha} + \frac{1}{A(M)}\frac{\partial M}{\partial\beta} = 0 \tag{3.7}$$

$$\frac{\partial\theta}{\partial\beta} - \frac{1}{M}\left(\frac{\partial A}{\partial M}\right)\frac{\partial M}{\partial\alpha} = 0. \tag{3.8}$$

In terms of Cartesian coordinates,

$$dy = M \sin\theta \, d\alpha + A \cos\theta \, d\beta \tag{3.9}$$

$$dx = M \cos\theta \, d\alpha - A \sin\theta \, d\beta. \tag{3.10}$$

Along the shock front ($\alpha = \text{const}$) we have

$$\frac{1}{A}\frac{\partial x}{\partial \beta} = -\sin\theta \tag{3.11}$$

$$\frac{1}{A}\frac{\partial y}{\partial \beta} = \cos\theta. \tag{3.12}$$

The Eqs. (3.7) and (3.8) may be written in characteristic form as

$$\left(\frac{\partial}{\partial \alpha} \pm C\frac{\partial}{\partial \beta}\right)\left(\theta \pm \int \frac{dM}{AC}\right) = 0, \tag{3.13}$$

where

$$C = \sqrt{-\frac{M}{AA'}} \tag{3.14}$$

and the prime denotes differentiation with respect to M.

In this form only derivatives in one direction appear, i.e., along the characteristic lines. Equation (3.13) represents waves moving in the direction of increasing and decreasing β with speed $\pm C$, respectively, where

$$\text{(i) on} \qquad \frac{d\beta}{d\alpha} = C, \qquad \theta + \int \frac{dM}{AC} = \text{const} \tag{3.15}$$

and

$$\text{(ii) on} \qquad \frac{d\beta}{d\alpha} = -C, \qquad \theta - \int \frac{dM}{AC} = \text{const}. \tag{3.16}$$

IV. Numerical Method of Characteristics

Consider two intersecting characteristics of opposite families in the $\alpha - \beta$ plane (See Fig. 4.1).

We denote by C^+ the characteristic with $d\beta/d\alpha = C$ and by C^- the characteristic with $d\beta/d\alpha = -C$, where $C > 0$. With the values of t, x, y, M and θ at points I and II, the method of characteristics is used to compute the corresponding values at the intersection point III.

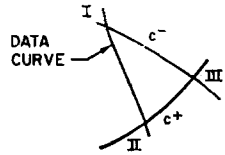

FIG. 4.1. Physical characteristics for the system of equations.

The characteristics themselves are given by $d\beta/d\alpha = \pm C$, so that, from Eq. (3.9) and (3.10) we obtain

$$dy = (M \sin\theta \pm N \cos\theta)\, d\alpha \tag{4.1}$$

$$dx = (M \cos\theta \pm N \sin\theta)\, d\alpha \tag{4.2}$$

where $N = AC$ or

$$N = \left[\frac{K}{2}(M^2 - 1)\right]^{1/2}.$$

The compatibility relations (3.13) may be expressed in the form

$$d\theta \pm (dM/N) = 0. \tag{4.3}$$

The above Eqs. (4.1), (4.2), and (4.3) constitutes six relations, which together with initial data and continuity conditions across the unknown free interface, may be resolved by the numerical method of characteristics.

Derivatives are replaced by finite differences and the following parameters are introduced:

$$P_y^- = (M \sin\theta - N \cos\theta) \cdot a \tag{4.4}$$

$$P_x^- = (M \cos\theta + N \sin\theta) \cdot a \tag{4.5}$$

$$P_y^+ = (M \sin\theta + N \cos\theta) \cdot a \tag{4.6}$$

$$P_x^+ = (M \cos\theta - N \sin\theta) \cdot a. \tag{4.7}$$

Using the above parameters given in Eqs. (4.4) to (4.7), Eqs. (4.1), (4.2), and (4.3) become

(i) along C^- characteristics:

$$y_{III} - y_I = \bar{P}_y^- \cdot (t_{III} - t_I) \tag{4.8}$$

$$x_{III} - x_I = \bar{P}_x^- \cdot (t_{III} - t_I) \tag{4.9}$$

$$\theta_{III} - \theta_I = -(M_{III} - M_I)/\bar{N}^- \tag{4.10}$$

(ii) along C^+ characteristics:

$$y_{III} - y_{II} = \bar{P}_y{}^+(t_{III} - t_{II}) \tag{4.11}$$

$$x_{III} - x_{II} = \bar{P}_x{}^+ \cdot (t_{III} - t_{II}) \tag{4.12}$$

$$\theta_{III} - \theta_{II} = -(M_{III} - M_{II})/\bar{N}^+ \tag{4.13}$$

where suffices $+$, $-$ refer to positive and negative characteristics C^+ (II, III) and C^- (I, III) respectively, and the bar superscript denotes a mean between end points II and III or I and III.

It will be necessary to use these mean values particularly in the calculation of the surface points.

4.1. *Calculation of Interface Points*

At the free surface the shocks must meet and travel together at the same velocity. For if one shock were to outdistance the other, then the pressure behind the faster shock would certainly exceed the pressure in front of the slower one. The conditions of continuity of pressure and normal-velocity across the free surface could not be satisfied, and a secondary wave would have to form to link the upper and lower shock fronts. We take this *secondary* wave as a segment of the diffracted shock front itself.

There is a jump in shock strength and shock inclination across the free surface. Hence, one must determine $M_{III_{u,l}}$ and $\theta_{III_{u,l}}$, referring to the values of shock Mach number and inclination at the surface point III in the upper and lower media, respectively (see Fig. 4.2).

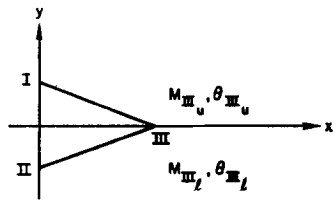

FIG. 4.2. Physical characteristics for the first surface point.

Surface points will be calculated at equal time intervals. The shock fronts in the upper and lower media must, of course, intersect on the undisturbed free surface, that is, at $y_{III} = 0$.

The calculation of the first surface point requires special treatment since a mathematical singularity exists at the free surface at $t = 0(x = 0)$.

The difficulty arises from the fact that although the two shocks must move together along the free surface, the initial conditions supplied by the preliminary

problem, which determined the initial strength of the transmitted shocks, do not permit this.

In fact, the condition required on the velocities of the two shocks at any surface point to ensure that the shocks travel together is

$$\frac{M_u a_u}{\cos \theta_u} = \frac{M_l a_l}{\cos \theta_l}. \tag{4.14}$$

It is clear that the shocks are still undistorted at time $t = 0$, so that their inclinations are $\theta_u = \theta_l = 0$. The Mach numbers of the initial transmitted shocks must then be in the inverse ratio of the sound speeds in their respective media. The condition is clearly overly restrictive. In the general case, the shocks will not move together at $t = 0$. This singularity, which is purely mathematical in nature, must be smoothed out in the shortest possible time interval, so that the velocities will be equal at all subsequent surface points.

With the physical condition $y_{III} = 0$ at interface, Eqs. (4.8) to (4.13) can be rewritten:

(i) along C^- characteristics as

$$-y_I = \bar{P}_y^-(t_{III} - t_I) \tag{4.15}$$

$$x_{III} - x_I = \bar{P}_x^-(t_{III} - t_I) \tag{4.16}$$

$$\theta_{III_u} - \theta_I = (M_{III_u} - M_I)/\bar{N}^- \tag{4.17}$$

(ii) along C^+ characteristics as

$$-y_{II} = \bar{P}_y^+(t_{III} - t_{II}) \tag{4.18}$$

$$x_{III} - x_{II} = \bar{P}_x^+(t_{III} - t_{II}) \tag{4.19}$$

$$\theta_{III_l} - \theta_{II} = -(M_{III_l} - M_{II})/\bar{N}^+. \tag{4.20}$$

where subscripts u and l denote the quantities in the upper and lower media, respectively.

From Eqs. (4.16) and (4.19) with $x_I = x_{II} = t_I = t_{II} = 0$, we obtain

$$\bar{P}_x^- = \bar{P}_x^+. \tag{4.21}$$

The functions 'P', as defined earlier, depend on Mach number M and inclination θ.

Eqs. (4.14), (4.17), (4.20), and (4.21) may then be solved simultaneously for the four unknowns M_{III_l}, M_{III_u}, θ_{III_u}, θ_{III_l} at the new surface point III. Having determined in this way the hodograph characteristics, the physical characteristics are calculated by specifying time t_{III} at which the shock reaches the particular point III on the undisturbed surface. Equations (4.16) and (4.19) then serve to determine the position of the surface point III.

The procedure for calculating subsequent surface points must be made more general.

One uses values of points I and II lying on the previous shock front (See Fig. 4.3). These points must be chosen so that the characteristic lines through them will intersect at a common point on the undistrubed free surface at a prespecified time. The procedure is necessarily iterative, since, for the general surface point, it is not possible to decouple the physical and hodograph characteristics from one another.

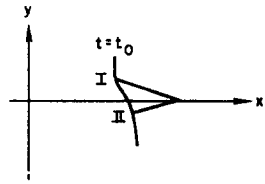

FIG. 4.3. Physical characteristics for a general surface point.

One chooses as points I and II, two points previously computed on the last shock front. The Eq. (4.14) for equality of velocity at the free surface, along with the two hodograph characteristic Eqs. (4.17) and (4.20) provide three relations for the four unknowns M_u, M_l, θ_u, and θ_l at point III. The remaining relation must come from the physical characteristics, which depend through the functions P upon the hodograph characteristics.

In this case, the physical and hodograph characteristics cannot be uncoupled from each other, due to the necessity of using averaged quantities along the characteristics, even for the first iteration. For even the smallest time steps there will be in general a significant difference between the Mach number at points I and II and at the corresponding point III above and below the interface, respectively, unless the two media are very similar in density and specific heat ratio.

The hodograph characteristics are determined approximately by estimating M_u or M_l at point III (the position of which is not yet known). Equations (4.17), (4.20), and (4.21) are sufficient to solve for the remaining variables θ_u, θ_l and the other Mach number M_{III}. The functions P may then be computed.

The value of time t_{III} at the new surface point is specified. Then, using the previously chosen values for points I and II, Equations (4.15) and (4.18), describing the physical characteristics in terms of the y-coordinate, will yield two values of the time t_{III} which may differ from the pre-selected value. Use this pre-selected value of t_{III} in Eqs. (4.15) and (4.18), new values of y are determined for adjusted points I and II along the previous shock front. Corresponding values of M, θ, t and x are obtained at these points I and II by interpolation along the shock front (see Fig. 4.4).

The solution of the three hodograph equations is repeated with a new estimate

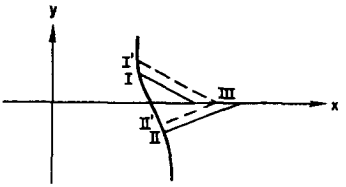

FIG. 4.4. Modification of data points I and II.

for M_u or M_l. After two or three iterations it is found that all conditions can be made compatible at the free surface. The coordinate x_{III} is found to agree to an accuracy of 0.1 % as calculated along either the C^+ or C^- characteristics from Eqs. (4.19) and (4.16), respectively.

4.2. *Calculation of Interior Points*

The computation of flow at points away from the free surface is considerably simpler. Here the hodograph characteristics, are only slightly coupled to the physical characteristics through the functions N which must be averaged along the C^+ and C^- characteristic directions. At the interior points, the time at point III is chosen equal to that for the corresponding shock front as computed at the free surface. In this way, the subsequent plotting of the shock front is facilitated.

For the first approximation, the functions N are evaluated for the known properties at points I, II only. Equations (4.17) and (4.20) may then be solved simultaneously for M_{III} and θ_{III}. The functions P are computed from Eqs. (4.4) to (4.7) and the position (x_{III}, y_{III}) of point III determined directly from C^+ characteristics (4.11) and (4.12) for the chosen time t_{III}. Equations (4.8) or (4.9) may provide an independent determination of t_{III} along the C^- characteristic. If these two values of t_{III} are not identical, then the data point farther from the free surface (point I in the upper medium or point II in the lower medium) is adjusted along the shock front and the computation repeated until the two values of t_{III} approach one another. Three iterations have been found sufficient.

The calculation of interior points is continued up to the boundary with the uniform region. In the uniform region convergence is immediate, thus signalling the completion of the calculations for that particular time t_{III}.

4.3. *Location of the Shock Front*

The procedure described for the calculation of M, θ, x, y for selected time intervals was developed specifically with a view to facilitating the task of plotting successive shock positions.

[redacted]

An alternate and considerably more laborious method of plotting the shock

profile would consist of tracing a smooth curve through points whose tangent directions θ_{III} are known. The first method was chosen as it avoids the necessity of a massive number of interpolations which would be required to locate a particular shock front, particularly in sensitive regions adjoining the uniform shock, where shock curvature changes rapidly. An independent check is still available by comparing selected points using both methods described above.

4.4. *Wave Pattern at the Free Surface*

The slopes and strengths of the diffracted shock fronts have now been determined on each side of the free surface. It remains to ensure that the free surface boundary conditions, i.e., continuity of pressure and normal particle velocity, are satisfied. This will not be the case unless a wave system is introduced behind the shock front. The primary question is that of determining which combination of compression and expansion waves is necessary. The problem has been studied in great detail by Henderson ([9], [10], [11]) in a series of articles dealing with shock refraction at gas interfaces. In these works, the flow is mapped simultaneously in the physical and hodograph planes. A particular wave pattern is deduced from a continuous evolution from a known pattern, either by numerical calculation, or graphically by gradual displacement of one shock polar representing the wave system in the upper medium relative to the corresponding shock polar in the lower medium. Some experimental work by Jahn [12] in a shock tube containing two gases separated by a very thin membrane was used as a basis of comparison. The methods described in these papers have the potential of systematic application to the present problem for all combinations of fluids. However, for the three fluid

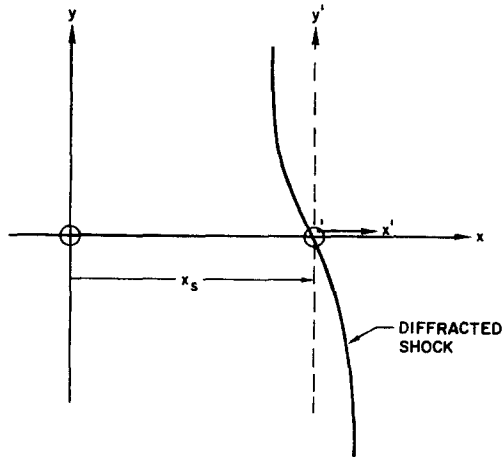

FIG. 4.5. Coordinate system fixed in moving shock.

combinations considered here, it was found after a few trials with various wave patterns that the conditions of continuity of pressure and velocity at the free surface could be satisfied simultaneously by introducing local expansion fans in both the upper and lower media immediately behind the diffracted shock front.

The flow field near the free surface is calculated in terms of a coordinate system (x', y') moving with the intersection point of the diffracted shock with the interface (Fig. 4.5).

The governing equations of fluid motion are

$$\begin{aligned} \frac{\partial u}{\partial t} + u\frac{\partial u}{\partial x} + v\frac{\partial u}{\partial y} &= -\frac{1}{\rho}\frac{\partial p}{\partial x} \\ \frac{\partial v}{\partial t} + u\frac{\partial v}{\partial x} + v\frac{\partial v}{\partial y} &= -\frac{1}{\rho}\frac{\partial p}{\partial y} \\ \frac{\partial \rho}{\partial t} + \frac{\partial \rho u}{\partial x} + \frac{\partial \rho v}{\partial y} &= 0 \\ \frac{\partial (p/\rho^\gamma)}{\partial t} + u\frac{\partial (p/\rho^\gamma)}{\partial x} + v\frac{\partial (p/\rho^\gamma)}{\partial y} &= 0. \end{aligned} \tag{4.22}$$

The first two equations represent conservation of momentum, the third conservation of mass, and the fourth the conservation of entropy along a streamline behind the shock front.

In terms of the moving coordinate system, these become

$$\begin{aligned} \frac{\partial (u_s + u')}{\partial t} + (u_s + u')\frac{\partial (u_s + u')}{\partial (x_s + x')} + v'\frac{\partial (u_s + u')}{\partial y'} &= -\frac{1}{\rho}\frac{\partial p}{\partial (x_s + x')} \\ \frac{\partial v'}{\partial t} + (u_s + u')\frac{\partial v'}{\partial (x_s + x')} + v'\frac{\partial v'}{\partial y'} &= -\frac{1}{\rho}\frac{\partial p}{\partial y'}. \\ \frac{\partial p}{\partial t} + (u_s + u')\frac{\partial \rho}{\partial (x_s + x')} + v'\frac{\partial \rho}{\partial y'} &= \rho\left(\frac{\partial (u' + u_s)}{\partial (x_s + x')} + \frac{\partial v'}{\partial y'}\right) \\ \frac{\partial (p/\rho^\gamma)}{\partial t} + (u_s + u')\frac{\partial (p/\rho^\gamma)}{\partial (x_s + x')} + v'\frac{\partial (p/\rho^\gamma)}{\partial y'} &= 0. \end{aligned} \tag{4.23}$$

Since no fundamental length or time parameter enters the problem, the equations may be expressed in terms of similarity variables

$$\bar{x} = \frac{x'}{u_{s_\infty} t}, \qquad \bar{y} = \frac{y'}{u_{s_\infty} t} \tag{4.24}$$

which reduces the problem to a quasi-steady two-dimensional form. The dependent variables are expressed in dimensionless form as:

$$\bar{u} = \frac{u'}{U_{s_\infty}}; \qquad \bar{v} = \frac{v'}{U_{s_\infty}} \tag{4.25}$$

$$\bar{p} = \frac{p}{\rho_0 U_{s_\infty}^2}; \qquad \bar{\rho} = \frac{\rho}{\rho_0}, \tag{4.26}$$

The transformation formulae from the moving frame (x', y', t) to the similarity coordinates $(\bar{x}, \bar{y})$ are

$$\begin{aligned} \frac{\partial}{\partial t} &= -\frac{(\bar{x} + \bar{x}_s)}{t}\frac{\partial}{\partial \bar{x}} - \frac{\bar{y}}{t}\frac{\partial}{\partial \bar{y}} \\ \frac{\partial}{\partial x'} &= \frac{1}{U_{s_\infty} t}\frac{\partial}{\partial \bar{x}} \\ \frac{\partial}{\partial y'} &= \frac{1}{U_{s_\infty} t}\frac{\partial}{\partial \bar{y}}. \end{aligned} \tag{4.27}$$

Using relations (4.24) to (4.27), and omitting the bar superscripts, Equations (4.23) reduce to

$$\begin{aligned} (x + x_s)\frac{\partial u}{\partial x} + y\frac{\partial u}{\partial y} - (u_s + u)\frac{\partial u}{\partial x} - v\frac{\partial u}{\partial y} &= \frac{1}{\rho}\frac{\partial p}{\partial x} \\ (x + x_s)\frac{\partial v}{\partial x} + y\frac{\partial v}{\partial y} - (u_s + u)\frac{\partial v}{\partial x} - v\frac{\partial v}{\partial y} &= \frac{1}{\rho}\frac{\partial p}{\partial y} \\ (x + x_s)\frac{\partial \rho}{\partial x} + y\frac{\partial \rho}{\partial y} - (u_s + u)\frac{\partial \rho}{\partial x} - v\frac{\partial \rho}{\partial y} &= \rho\left(\frac{\partial u}{\partial x} + \frac{\partial v}{\partial y}\right) \\ (x + x_s)\frac{\partial p}{\partial x} + y\frac{\partial p}{\partial y} - (u_s + u)\frac{\partial p}{\partial x} - v\frac{\partial p}{\partial y} & \\ = a^2\left[(x + x_s)\frac{\partial \rho}{\partial x} + y\frac{\partial \rho}{\partial y} - (u_s + u)\frac{\partial \rho}{\partial x} - v\frac{\partial \rho}{\partial y}\right] & \end{aligned} \tag{4.28}$$

where a is the sound speed.

The equations are now transformed to polar coordinates (r, ϕ) about the origin O' fixed in the shock. The angle ϕ is measured anticlockwise from the positive y axis, so that

$$x = -r\sin\phi, \qquad y = r\cos\phi, \qquad \phi = \tan^{-1}(-x/y).$$

Then derivatives transform as

$$\frac{\partial}{\partial x} = -\frac{1}{r}\left(r \sin \phi \frac{\partial}{\partial r} + \cos \phi \frac{\partial}{\partial \phi}\right)$$
$$\frac{\partial}{\partial y} = \frac{1}{r}\left(r \cos \phi \frac{\partial}{\partial r} - \sin \phi \frac{\partial}{\partial \phi}\right). \tag{4.29}$$

The limiting form of the Eqs. (4.28) under the transformation (4.29) as $r \to 0$; i.e., in the immediate neighborhood of the shock front-free surface intersection, is

$$\rho\{[x_s - (u_s + u)] \cos \phi - v \sin \phi\} \frac{du}{d\phi} = \cos \phi \frac{dp}{d\phi}$$
$$\rho\{[x_s - (u_s + u)] \cos \phi - v \sin \phi\} \frac{dv}{d\phi} = \sin \phi \frac{dp}{d\phi}$$
$$\{[x_s - (u_s + u)] \cos \phi - v \sin \phi\} \frac{d\rho}{d\phi} = \rho\left(\cos \phi \frac{du}{d\phi} + \sin \phi \frac{dv}{d\phi}\right) \tag{4.30}$$
$$\{[x_s - (u_s + u)] \cos \phi - v \sin \phi\} \frac{dp}{d\phi} = a^2\{[x_s - (u_s + u)] \cos \phi - v \sin \phi\} \frac{d\rho}{d\phi}.$$

Equations (4.30) are integrated numerically, starting from the shock front and progressing towards the free surface in both the upper and lower media. The wave pattern corresponds to two expansion fans. The tails of these fans are chosen specifically to match simultaneously the pressure and normal particle velocity. In this wave the slope of the disturbed interface behind the shock front is determined.

4.5. *Shape of the Head Characteristics*

As the shock front sweeps along the interface, the fluid pressure will rise suddenly. Upon the passage of the shock through each point on the free surface, that point becomes a source of an expansion wave which spreads out into the uniform flow region, carrying the first message of the interface disturbance. These waves form an envelope which will be termed the head characteristic. The equation of this envelope may be determined from an examination of the general flow equations (4.29) expressed in a reference frame moving with the shock front.

From the calculations for the shock shape, it was observed that the velocity u_s of the shock along the free surface was nearly constant (Fig. 5.6). This information may be used to simplify the governing equations, since, if $u_s = \text{const}$, then

$$x_s = u_s t$$

and in dimensionless variables

$$\bar{x}_s \equiv \frac{x_s}{U_{s_\infty} t} = \frac{u_s}{U_{s_\infty}} \equiv \bar{u}_s . \tag{4.31}$$

Equations (4.29) reduce to

$$\begin{aligned}
(x-u)\frac{\partial u}{\partial x} + (y-v)\frac{\partial u}{\partial y} &= \frac{1}{\rho}\frac{\partial p}{\partial x} = K\gamma\rho^{\gamma-2}\frac{\partial \rho}{\partial x} \\
(x-u)\frac{\partial v}{\partial x} + (y-v)\frac{\partial v}{\partial y} &= \frac{1}{\rho}\frac{\partial p}{\partial y} = K\gamma\rho^{\gamma-2}\frac{\partial \rho}{\partial y} \\
(x-u)\frac{\partial \rho}{\partial x} + (y-v)\frac{\partial \rho}{\partial y} &= \rho\left(\frac{\partial u}{\partial x} + \frac{\partial v}{\partial y}\right)
\end{aligned} \tag{4.32}$$

where $p = K\rho^\gamma$ has been used to eliminate the pressure in favor of the density. The characteristics of this homogeneous set of equations are independent of velocity and density and are represented by

$$\frac{dy}{dx} = \frac{y^2 - a^2}{(x-u)\,y \pm a[(x-u)^2 + y^2 - a^2]^{1/2}} . \tag{4.33}$$

Equations (4.33) have been integrated numerically, with initial conditions being those on the shock front at the boundary between the diffracted and uniform segments of the shock.

The characteristics were found to be very nearly straight lines. The time interval between the passage of the shock and the arrival of the head characteristic represents the period during which a fluid particle is subjected to the full pressure behind the shock front. Upon the arrival of the characteristic, the pressure begins to fall toward its original level.

V. Results and Discussion

Computations have been completed for three cases, in which the difference in initial shock velocities between the upper and lower media varied between 8%, 22%, and 26%. The results are qualitatively similar over this range and will be discussed collectively in terms of the 26% case.

The initial conditions are shown in Fig. 5.1 in which are represented the initial uniform shock front for $t < 0$ and the uniform transmitted shocks in the upper and lower media for $t = 0$. Waves reflected into the region $x < 0$ will not influence the propagation and local diffraction of the transmitted shock waves.

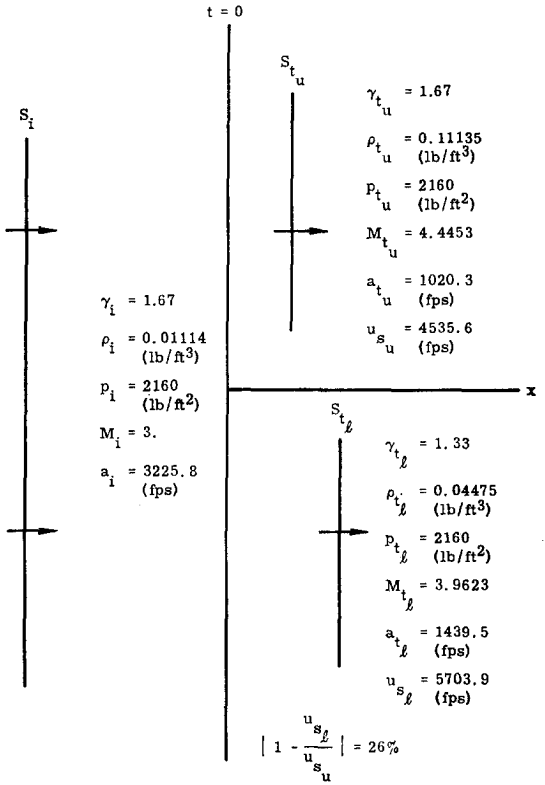

FIG. 5.1. Initial and transmitted shock wave at time $t = 0$ (26 % difference in shock velocities).

The shock shapes are plotted in the physical plane in Fig. 5.2. In all three cases, the shock fronts are seen to bend markedly at the boundary between the uniform and disturbed flow regions and at the free surface $y = 0$. The portions of the diffracted shock front between these regions are almost plane and uniform. In addition, the surfaces separating the uniform and disturbed flow regions are very nearly plane, suggesting a self-similar property of the flow, which one would expect on the basis of dimensional analysis. Since no length or time scale may be formed by any combination of the input parameters, the solution may be shown to depend not on x, y, t separately, but rather on similarity variables proportional to $(x/t, y/t)$.

When the shock profiles are replotted in terms of the new variables, they are found in Fig. 5.3 to fall very nearly onto one universal curve. In other words, the shock shapes are affine, their shape remains unchanged and only their scale increases in time. It will be noted however that the shock profiles corresponding to earlier times $t = 2, 3, 4 \times 10^{-4}$ seconds depart most from this common curve, indicating

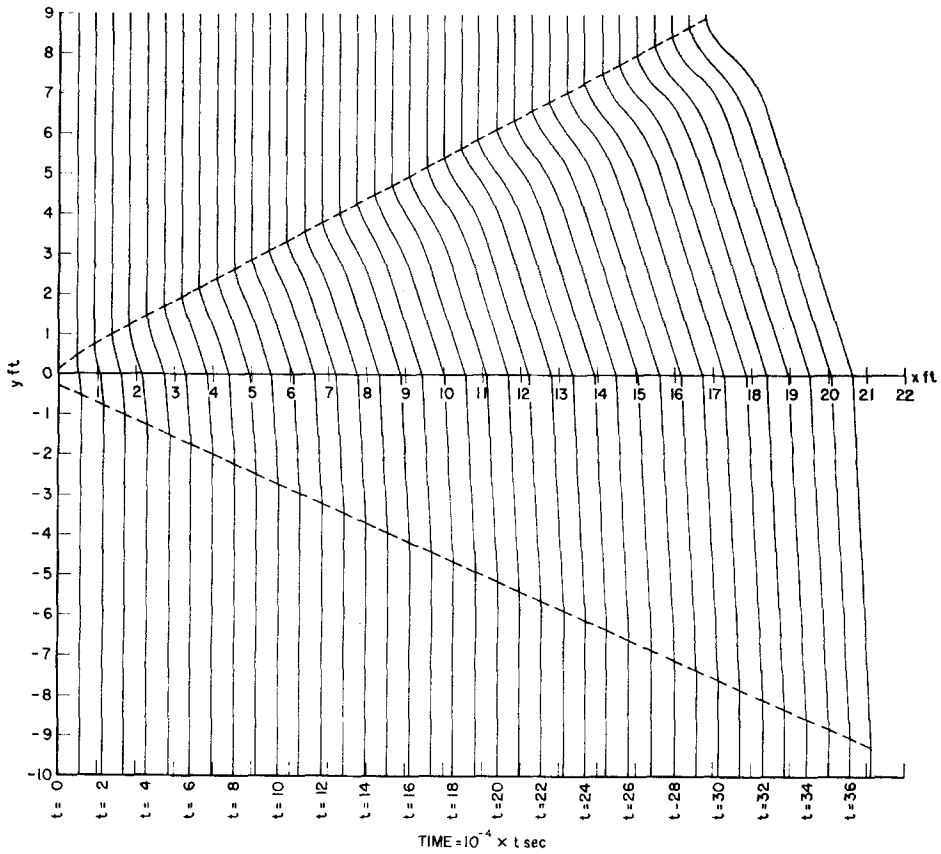

FIG. 5.2. The shock shape in physical coordinates (x, y) (26 % difference in shock velocities).

that a self-similar solution is not obtained immediately from $t = 0$. Fig. 5.4 shows more details of the approach to similarity for early times.

An estimate of the length of the *transition* period to self-similar behavior is obtained most effectively through a plot of the boundary of the disturbed region as shown in Fig. 5.5.

Straight lines in the physical plane must correspond to lines of constant y/t in the similarity plane, since lines of constant y/x imply lines of constant y/t, x/t, where time t plays the rôle of a parameter. There appears to be an adjustment period of about 12×10^{-4} seconds, the delay being due to smoothing of the mathematical singularity at the free surface at time $t = 0$.

The shock velocity at the free surface (component directed along the undisturbed free surface) is plotted in Fig. 5.6.

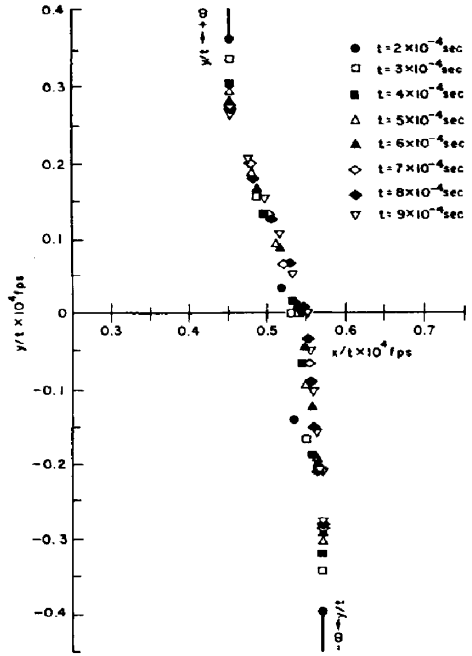

FIG. 5.3. The shock shape in similarity coordinates $(x/t, y/t)$ for the earlier times (26 % difference in shock velocities).

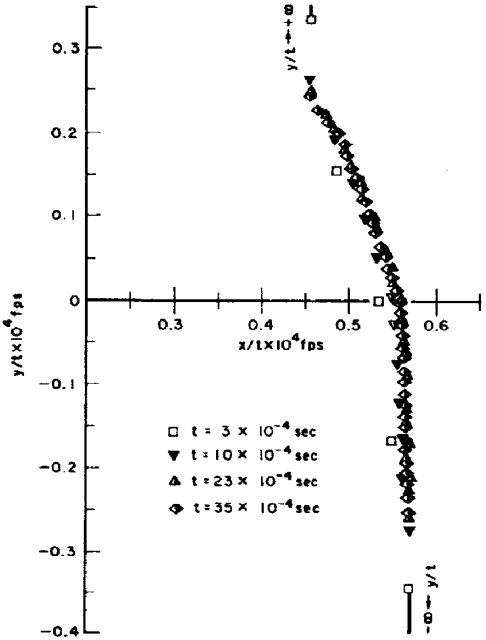

FIG. 5.4. The shock shape in similarity coordinates $(x/t, y/t)$ for the early, intermediate and late times (26 % difference in shock velocities).

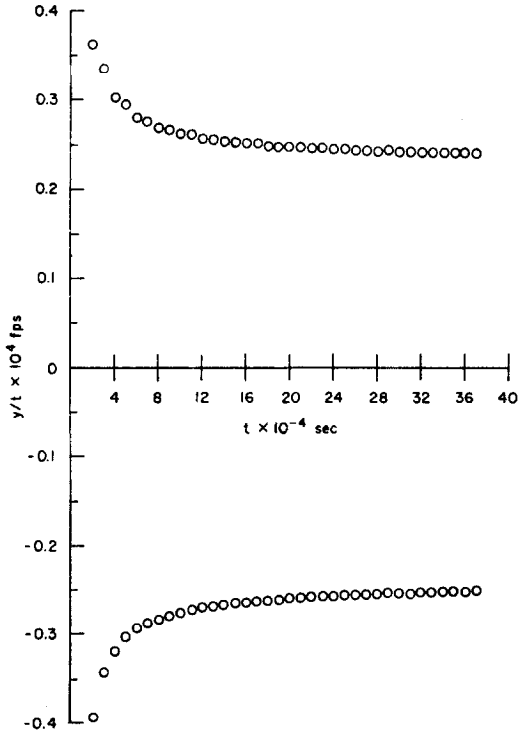

FIG. 5.5. The width of the disturbed region as a function of time (26 % difference in shock velocities).

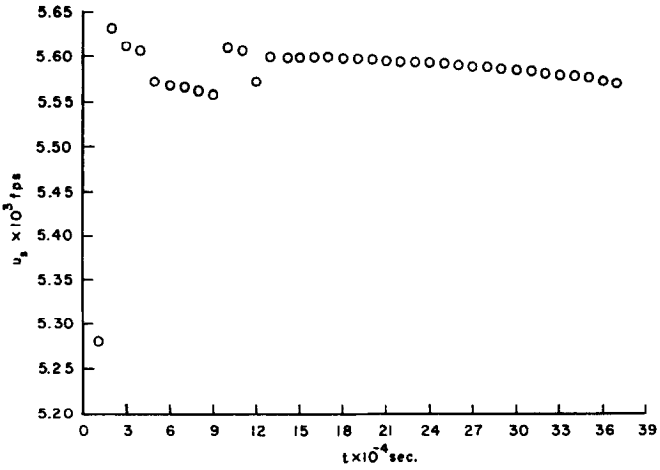

FIG. 5.6. The surface shock velocity parallel to the undisturbed free surface as a function of time (26 % difference in shock velocities).

The shock front sweeps over the free surface at velocities which vary in a narrow band of only $\pm 0.5\%$.

The horizontal components of fluid velocity behind the shock front are plotted in Figure 5.7. Fluid velocities are very nearly constant, again confirming that the diffracted portions of the shock front between the free surface and the undisturbed boundary are almost uniform. The vertical components of fluid velocity are shown in Figure 5.8. At the free surface $y = 0$, the boundary conditions require that the normal components of velocity be continuous. This will be achieved physically through a pair of expansion fans immediately behind the upper and lower shocks at the free surface, without influencing significantly the velocity distributions on either side of the free surface.

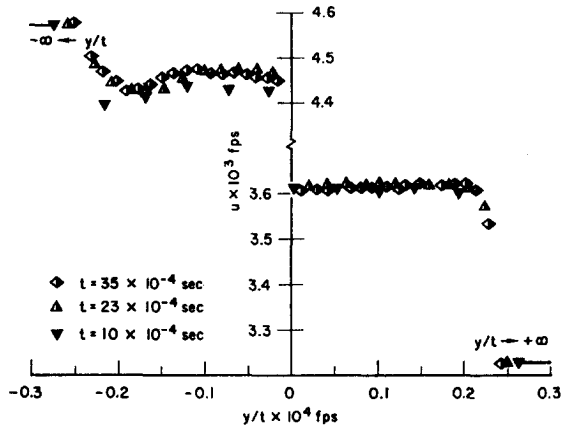

FIG. 5.7. The horizontal component of fluid velocity behind the shock front in terms of similarity variable of y/t (26 % difference in shock velocities).

In the same manner, the pressure distributions behind the shock front, plotted in Figure 5.9, will be made continuous at $y = 0$ by the insertion of appropriate expansion fans.

The density distribution along the shock front, shown in Fig. 5.10, is uniform except for rapid changes occuring at the free surface and in the region where the diffracted portion of the shock merges into the uniform shock front.

The variation of the pressure, velocity, and density behind the shock front as it passes across the free surface ($y = 0$) is determined from the detailed analysis of the flow patterns behind the shock described in Section 4.4. The results of the matching procedure are shown in Fig. 5.11. The pressure variation and streamline direction at each point in the expansion in the upper and lower media are plotted as functions of angle. The solution is shown by the dashed lines in terms of the

unique combination of expansion fan angles which permit equality of pressures and streamline directions in both fluids.

The head characteristics, representing the first waves penetrating into the uniform region behind the undisturbed shock, are plotted in Fig. 5.12. They appear very nearly as plane reflected waves in the vicinity of the shock front.

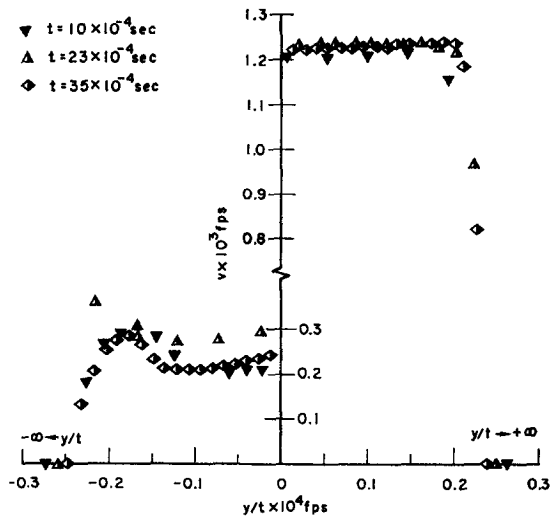

FIG. 5.8. The vertical component of fluid velocity behind the shock front in terms of similarity variable of y/t (26 % difference in shock velocities).

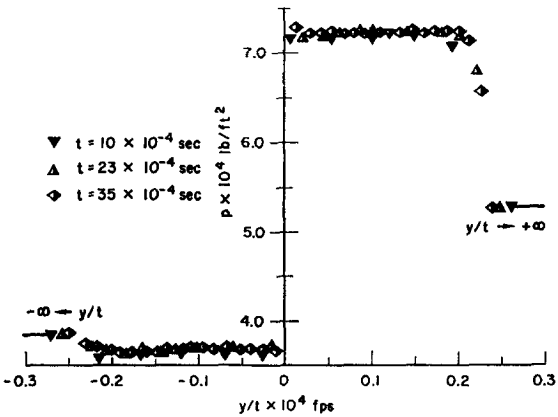

FIG. 5.9. The pressure distribution behind the shock front in terms of similarity variable of y/t (26 % difference in shock velocities).

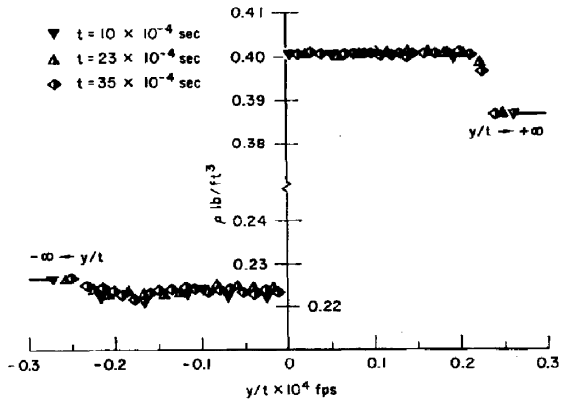

FIG. 5.10. The density distribution behind the shock front in terms of similarity variable of y/t (26 % difference in shock velocities).

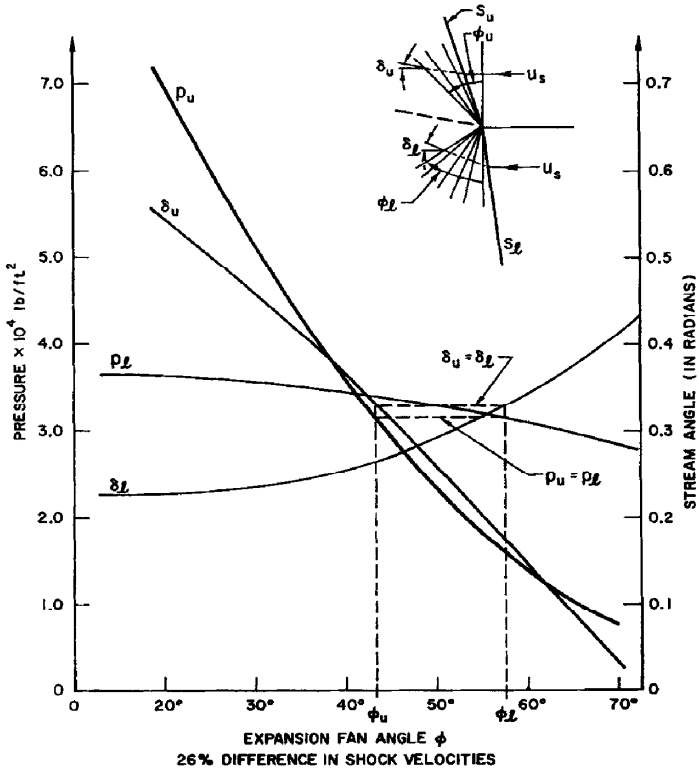

FIG. 5.11. Wave pattern behind shock front at disturbed interface (26 % difference in shock velocities).

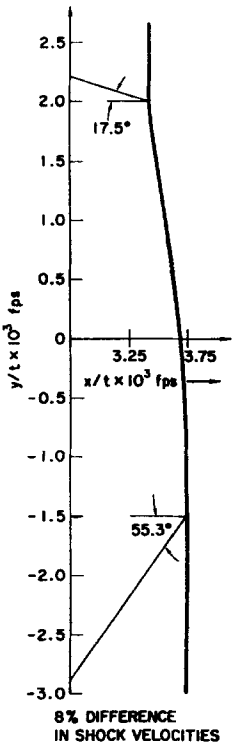

FIG. 5.12. Head characteristics in vicinity of shock front.

The accuracy of the method has been examined by Chisnell for converging cylindrical and spherical shocks and by Bird [1] for the simple problem of a plane shock front moving into a stratified medium whose layers run parallel to the incident shock. In these cases no shock diffraction occurs. Chisnell found uncannily high accuracy when compared with the similarity solutions of Guderley [8]. Bird compared the Chisnell–Whitham method with a method of characteristics solution for the plane shock problem, and found that highest accuracy was obtained for combinations of weak shock waves and favorable (positive) density profiles in a gas with a high ratio of specific heats. It is not clear that specific conclusions may be extrapolated to the present more general problem. Nonetheless the study points out the importance of the effect of wave reflection far downstream on the evolution of the shock front.

The calculations show that the complete flow field may be determined by these methods for differences in shock velocities up to about 30%. For greater differences, as would surely be the case for blast waves at an air-water interface, it becomes apparent that the reflected wave pattern behind the shock at the free surface takes

on increasing importance to the point that the basic assumptions inherent in

simultaneously with the wave pattern behind the shock front.

VI. Conclusions

The method of characteristics based on Whitham's technique has been applied for the first time to the interaction of shock waves with a free surface. Shock diffraction may be computed for waves of arbitrary strength, provided that the dissimilarity between the two media adjoining the free surface does not result in shock velocities at $y = \pm\infty$ which differ by more than 30%. Greater degrees of shock diffraction will be accompanied by reflected and re-reflected waves which may overtake the shock front. These effects have not been included in Whitham's technique in which changes in shock Mach number are related only to local variations in *ray* tube cross-sectional area.

The problem considered is known to possess the property of self-similarity. The numerical calculations indicate a rapid approach to self-similar profiles in a time interval of about 1.2 milliseconds, the delay being due to the initial mathematical singularity at the free surface.

The technique is directly applicable to shock wave diffraction at an ocean surface and will be extended in future work to include the effects of stratification on either side of the interface, as a means of investigating shock wave propagation over large depths in the oceans and upper atmosphere.

Acknowledgments

The authors thank W. Chester, L. F. Henderson, and G. B. Whitham for helpful discussions. This study was supported by the Office of Naval Research.

References

1. G. A. Bird, The motion of shock-wave through a region of nonuniform density, *J. Fluid Mech.* **11** (1961), 180–186.
2. W. Chester, The propagation of shock waves in a channel of non-uniform width, *Quart. J. Mech. Appl. Math.* **6** (1953), 440.
3. W. Chester, The quasi-cylindrical shock tube, *Phil. Mag.* **45** (1954), 1293.
4. R. F. Chisnell, The motion of a shock wave in a channel, with applications to cylindrical and spherical shock waves, *J. Fluid Mech.* **2** (1957), 286–298.

5. R. COLLINS AND M. HOLT, Intense explosions at the ocean surface, *Phys. of Fluids* **11** (1968), 701–713.
6. R. COURANT AND K. FRIEDRICHS, "Supersonic Flow and Shock Waves," pp. 176–181, Interscience, New York, 1948.
7. A. I. GUBANOV, Reflection and refraction of shock waves at the boundary of two media, *J. Tech. Phys.*, XXVIII, No. 9, Series B (1958), 2035–2040 (in Russian).
8. G. GUDERLEY, *Luftfahrtforschung* **19** (1942), 302.
9. L. F. HENDERSON, The refraction of a plane shock wave at a gas interface, *J. Fluid Mech.* **26** (1966), 607–637.
10. L. F. HENDERSON, On expansion waves generated by the refraction of a plane shock at a gas interface, *J. Fluid Mech.* **30** (1967), Pt. 2, 385–402.
11. L. F. HENDERSON AND A. K. MACPHERSON, On the irregular refraction of a plane shock wave at a mach number interface, *J. Fluid Mech.* **32** (1968), Pt. 1, 185–202.
12. R. G. JAHN, Refraction of shock waves from a gaseous interface, *J. Fluid Mech.* **1** (1956), 457.
13. D. C. PACK, The reflexion and diffraction of shock waves, *J. of Fluid Mech.* **18** (1963), 549–576.
14. S. PATERSON, The reflection of a plane shock wave at a gaseous interface, *Proc. Phys. Soc.* **61** (1948), 119–121.
15. H. POLACHEK AND R. J. SEEGER, On shock-wave phenomena; Refraction of shock waves at a gaseous interface, *Phys. Rev.* **84** (1951), 922–929.
16. P. M. STOCKER AND D. S. BUTLER, "Refraction of a Shock Wave by a Heated Layer," Part I: Continuous Temperature Gradient. *ARDE* Report (B) 7/57, 1957.
17. G. P. TALBOT, "Shock Bifurcation in a Heated Layer," *ARDE* Report (B) 23/58, 1958.
18. G. B. WHITHAM, On the propagation of shock waves through regions of non-uniform area or flow, *J. Fluid Mech.* **4** (1958), 337–360.